International Journal of Concrete Structures and Materials
DOI 10.1186/s40069-018-0264-5
ISSN 1976-0485 / eISSN 2234-1315

Durability of Mortar Incorporating Ferronickel Slag Aggregate and Supplementary Cementitious Materials Subjected to Wet–Dry Cycles

Ashish Kumer Saha* and Prabir Kumar Sarker

(Received August 31, 2017, Accepted November 10, 2017)

Abstract: This paper presents the strength and durability of cement mortars using 0–100% ferronickel slag (FNS) as replacement of natural sand and 30% fly ash or ground granulated blast furnace slag (GGBFS) as cement replacement. The maximum mortar compressive strength was achieved with 50% sand replacement by FNS. Durability was evaluated by the changes in compressive strength and mass of mortar specimens after 28 cycles of alternate wetting at 23 °C and drying at 110 °C. Strength loss increased by the increase of FNS content with marginal increases in the mass loss. Though a maximum strength loss of up to 26% was observed, the values were only 3–9% for 25–100% FNS contents in the mixtures containing 30% fly ash. The XRD data showed that the pozzolanic reaction of fly ash helped to reduce the strength loss caused by wet–dry cycles. Overall, the volume of permeable voids (VPV) and performance in wet–dry cycles for 50% FNS and 30% fly ash were better than those for 100% OPC and natural sand.

Keywords: ferronickel slag, fly ash, blast furnace slag, compressive strength, wet–dry cycle, porosity.

1. Introduction

Substantial amounts of industrial by-products are currently used worldwide as construction materials. Nevertheless, it is important to increase recycling of the unused by-products in order to reduce the volume of waste causing environmental pollution, to save the huge area of land occupied by them and to reduce the depletion of natural resources. Concrete is the most widely used construction material in the world and it has a significant contribution to the greenhouse gas emissions. Thus, utilisation of the currently available industrial by-products in manufacture of concrete can significantly improve sustainability of the construction sector. Different types of granulated slags are produced as by-products in processing of minerals. A considerable amount of research is available in literature on the utilisation of these granulated slags as replacement of natural aggregate and ground slag as replacement of cement. The most common type of commercially available ground slag is GGBFS (Hooton 2000; Shafigh et al. 2013; Yang et al. 2017). Durability improvement of concrete by the use of GGBFS as an SCM has been well documented by many works in literature (Siddique and Khan 2011; Safiuddin et al. 2010; Kim et al. 2016). While ground slags can be used as partial replacement of cement, the binder usually occupies only 15–20% volume of concrete, and slags cannot be used as full replacement of cement (Roychand et al. 2016). Since aggregates occupy a much larger volume fraction in concrete or mortar, the use of granulated slag as aggregate can substantially increase its usage. In addition, use of granulated slags as aggregate do not require grinding that can save cost and energy. Furthermore, the demand of natural sand as fine aggregate is increasing fast in many countries. Since river sand is the most common fine aggregate, uncontrolled river dredging is occurring in different parts of the world (Preciso et al. 2012; Davis et al. 2000). Extensive sand mining from river bed can cause severe disruption of the aquatic ecosystem (Padmalal et al. 2008). Therefore, the use of granulated slag by-products can be considered as a cost-effective and environmentally friendly alternative to natural sand for concrete production.

Among different types of slag aggregates, coal bottom ash (CBA), steel slag, copper slag and FNS are the most frequently studied materials because they are produced in considerable quantities. Aggregate plays a vital role on all concrete properties such as workability, strength and durability. The use of coal bottom ash as fine aggregate was found to reduce compressive and tensile strengths of concrete after the initial curing period. However, strength is usually increased at the later ages by pozzolanic reaction of CBA (Yüksel et al. 2011). Durability properties of CBA concrete such as drying shrinkage and freeze–thaw resistance were reported to improve as compared to the control specimens (Bai et al. 2005). However, the resistance to wet–dry cycle of CBA concrete was poor due to high porosity of

Department of Civil Engineering, Curtin University, Perth, WA 6845, Australia.
*Corresponding Author;
E-mail: a.saha@postgrad.curtin.edu.au

Published online: 26 March 2018

ash (Aggarwal et al. 2007; Ghafoori and Bucholc 1996). The use of steel slag or electric arc furnace (EAF) slag in concrete was found to significantly reduce workability (Etxeberria et al. 2010; Manso et al. 2004). Mechanical properties of concrete such as compressive strength, splitting tensile strength, flexural strength and modulus of elasticity were reported to improve by the use of EAF slag (Al-Negheimish and Al-Zaid 1997; Qasrawi et al. 2009). The improvement of mechanical properties is attributed to the higher angularity and roughness of aggregate particles that can improve bonding between cement paste and aggregate (Maslehuddin et al. 2003). However, strength losses of concrete in accelerated ageing and freeze–thaw exposures were higher for steel slag aggregate as compared to natural aggregate. Over 25% loss of compressive strength was observed in steel slag aggregate concrete by the exposure to wet–dry cycles. The poor performance of EAF slag was attributed to the presence of pernicious free lime and periclase in the slag (Manso et al. 2006; Pellegrino and Gaddo 2009). Improvements of the hardened properties of concrete such as compressive strength, tensile strength and abrasion resistance by partial replacement of fine aggregate with the copper slag have been reported in the literature (Al-Jabri et al. 2011; Wu et al. 2010; Brindha and Nagan 2011). Durability properties such as sulphate resistance and carbonation resistance of concrete with copper slag aggregate were reported to be identical to those of the control specimens (Ayano and Sakata 2000). However, the freeze–thaw resistance of copper slag concrete was poor due to excessive bleeding that caused internal defects in the samples (Shoya et al. 1997).

Production of ferronickel alloys produces a large quantity of FNS as by-product (Saha and Sarker 2016). Currently, limited quantities of this FNS is utilised in local construction works. Figure 1 shows an example of the utilisation of FNS aggregate as 30% replacement of natural sand in concrete breakwaters in New Caledonia (Saha and Sarker 2017a). Although the nickel producers supply FNS locally for using as fine aggregate, the properties of FNS aggregate concrete is scarce in literature. Moreover, the physical and chemical properties of FNS can vary significantly with the type of source ore, smelting temperature and cooling method.

Fig. 1 Breakwaters of concrete with 30% ferronickel slag aggregate in marine exposure for 20 years.

Laterite, garnierite and pentlandite ores are some primary sources of nickel. The ore is usually smelted at a high temperature that produces the molten slag as by-product. The molten slag can be granulated by air or water (JSCE Committee 1994). Very limited studies available in literature show that FNS can be used as an alternative fine aggregate in concrete (Sakoi et al. 2013). It was shown that workability decreased and bleeding increased by the use of FNS aggregate in concrete due to its high unit weight (JIMA 1991; Shoya et al. 1999; Sato et al. 2011). The hardened concrete properties such as compressive strength, modulus of elasticity and tensile strength were improved by the partial replacement of sand with FNS. Improvement of these mechanical properties was attributed to the physical properties of FNS such as high unit weight, well-grading and angularity of the particle, which improved bonding between paste and aggregates (Sakoi et al. 2013; Shoya et al. 1999). Among the limited literature available on durability properties of FNS aggregate concrete, Shoya et al. (1999) showed that 50% replacement of natural aggregate by FNS resulted in better freeze–thaw resistance as compared to the control specimens. On the other hand, Shoya et al. (2003) reported better frost resistance of concrete containing FNS aggregate. However, Tomosawa et al. (1997) observed alkali–silica reaction associated with FNS aggregates and suggested the use of fly ash or blast furnace slag as partial replacement of cement as a mitigation. The above studies used FNS aggregates collected from the slow cooling pits.

This paper evaluates the strength and durability of cement mortar using FNS fine aggregate produced by smelting of garnierite ore at a temperature between 1500 and 1600 °C (Rahman et al. 2017). The molten slag is granulated by rapid cooling using seawater. The FNS is characterised by relatively high magnesium content as compared to the FNS utilised in the previous studies (Wang et al. 2011; Kang et al. 2014; Choi and Choi 2015). Thus, the source ore and granulation method of this FNS are different from those used in the studies available in literature. About 12–14 tonnes of FNS is produced as by-product in the production process of one tonne of ferronickel alloy. The annual FNS production of the smelter is estimated as 1.7 million tonnes. The current deposit of FNS in the premises of the smelter is about 25 million tonnes despite its various uses by the local construction industries. The potential alkali–silica reaction (ASR) of the FNS and the effectiveness of SCMs such as fly ash and GGBFS as ASR mitigating measure was studied in our ongoing work (Saha and Sarker 2016). This paper presents the strength development of mortars containing different percentages of FNS with or without fly ash and GGBFS as cement replacement. Further to the strength development in normal environmental condition, it is also important to have knowledge on the durability of a construction material when exposed to seasonal variations and aggressive environments. Thus, the long-term durability of mortar specimens was evaluated in terms of volume of permeable voids and the changes in mass and strength after exposure to an accelerated weathering condition represented by alternate cycles of wetting and drying at 110 °C. The

mineralogical phases of the specimens after the wet–dry cycles were studied in order to understand the effects of FNS and SCMs.

2. Experimental Work

2.1 Materials

Commercial ordinary Portland cement (OPC) was used as the main binder in this study. A class F fly ash and GGBFS were used as supplementary cementitious materials. FNS was used as a replacement of natural sand in the form as it was received from the smelter without any processing. Table 1 shows the chemical compositions of these materials as determined by X-Ray Fluorescence (XRF) test. It can be seen that majority of the FNS constituents are Silicon, Magnesium and Iron. The Calcium contents of OPC and GGBFS are much higher than that of the fly ash (0.27%). On the other hand, the main constituents of fly ash were silica (76.34%) and alumina (14.72%). Table 2 presents the physical properties of the binders.

Figure 2 shows the physical appearance of FNS fine aggregate and natural sand used in this study. It can be seen that FNS is angular in shape with much more coarser particles as compared to natural sand.

The grading curves of fine aggregates combining different percentages of FNS and natural sand are shown in Fig. 3. The upper and lower limits of fine aggregates recommended by the Australian Standard AS 2758.1 (1998) are also shown in the figure. It can be seen that while most of the combinations are within the limits of the Standard, the grading curve of 100% FNS is slightly below the lower limit because of the lack of fine particles in FNS. Thus, the size distribution of fine aggregate was improved by combining FNS with natural sand. It can be seen that the mix of 50% FNS and 50% natural sand has resulted in a well-graded combination, which includes particles of different sizes and shapes.

As given in Table 3, the fineness modulus of FNS was 4.07 and that of natural sand was 1.95. The unit weights of FNS and natural sand were 2780 and 2160 kg/m^3, respectively. The water absorptions of FNS and sand were 0.42 and 0.35%, respectively.

2.2 Mixture Proportions and Test Methods

The mixture proportions of mortars used in this study are given in Table 4. FNS aggregate was used to replace natural sand by 0, 25, 50, 75 and 100% in the mortar mixtures. Previous studies showed that FNS aggregates may potentially cause alkali–silica reaction (ASR). Therefore, fly ash and GGBFS were used as 30% replacement of cement. This measure was found to substantially reduce the expansion due to ASR in our ongoing study (Saha and Sarker 2016). A total of 15 mixtures in three series of the binder compositions were investigated: 100% OPC, 30% cement replacement by fly ash and 30% cement replacement by GGBFS. In Table 4, the designation of a mixture starts with PC for 100% OPC, FA for 30% fly ash or BFS for 30% GGBFS. The number at

Table 1 Chemical compositions and loss on ignition (LOI) of OPC, FNS, fly ash and GGBFS (mass%).

Material	OPC	FNS	Fly ash	GGBFS
CaO	63.11	0.42	0.6	41.22
SiO_2	20.29	53.29	76.34	32.45
Al_2O_3	5.48	2.67	14.72	13.56
MgO	1.24	31.6	0.54	5.1
Fe_2O_3	2.85	11.9	3.69	0.82
SO_3	2.49	–	0.11	3.2
Na_2O	0.29	0.11	0.19	0.27
K_2O	0.45	–	0.96	0.35
Cr_2O_3	0.02	1.08	–	–
P_2O_5	0.17	–	0.1	0.03
SrO	0.05	–	–	–
TiO_2	0.27	–	0.61	0.49
Mn_2O_3	0.08	–	0.07	0.25
ZnO	0.04	–	–	–
NiO	–	0.1	–	–
Co_3O_4	–	0.01	–	–
LOI[a]	3.39	0.83	0.53	1.11

[a]Loss on ignition.

Table 2 Physical properties of binders.

Material	Specific surface area (m^2/kg)	Specific gravity
OPC	337	3.16
Fly ash	330	2.20
GGBFS	450	2.90

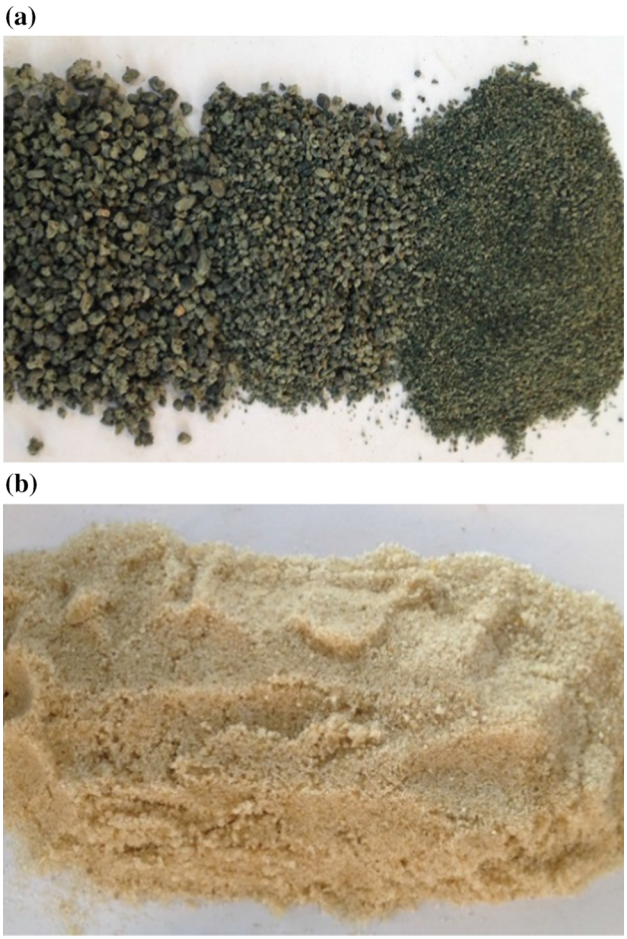

Fig. 2 a Ferronickel slag aggregate and b natural sand.

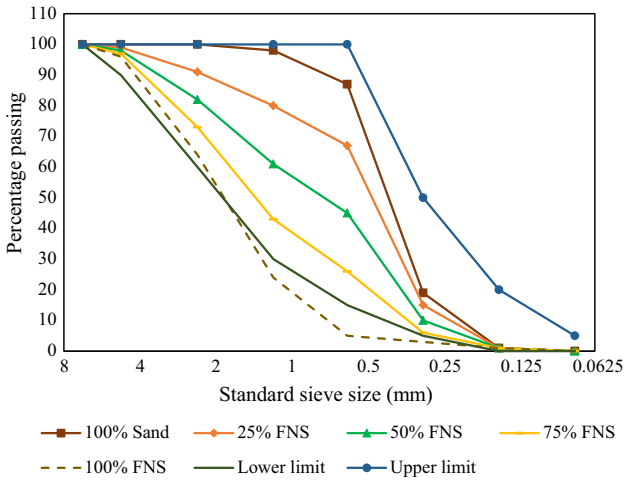

Fig. 3 Gradation of fine aggregates combining FNS and natural sand.

the end of a mix designation represents the percentage of FNS in fine aggregate.

Cube specimens of 50 mm sides were cast using freshly mixed mortar. The specimens were demolded at 24 h after casting and then cured in lime saturated water up to 28 days. Compressive strength tests were conducted at 3, 7, 28, and 56 days of age. Three specimens were tested at each age and an average value of the compressive strength is reported. The tests were conducted at a loading rate of 0.333 MPa/s.

In order to determine porosity of the samples, volume of permeable voids (VPV) test was conducted on the 50 mm mortar cubes in accordance with the ASTM C 642 (2006) standard. The test consists of measurements of masses of the sample in oven-dry condition, saturated surface dry condition, immersed in water and after subjecting to boiling condition. At first, the samples were dried in an oven at 110 °C for 24 h and then cooled down to room temperature for 3 h to record the dry mass. The samples were then submerged in water for 48 h and the immersed mass was recorded. The saturated surface dry mass was measured after moving the samples out from the water. The samples were then boiled in water for 5 h, cooled down and the boiled mass was recorded. Volume of the permeable voids was calculated using the values of these masses.

The specimens were exposed to cycles of alternate drying at 110 °C and wetting at 23 °C in order to evaluate their resistance to an accelerated weathering condition. This exposure condition is considered to accelerate the possible degradation of mortar by seasonal variations of wetting–drying and heating–cooling by surrounding environment over the age. The specimens were cured in water at 23 °C for 28 days before beginning of the alternate wet–dry cycles. One cycle of the exposure consisted of drying the specimen at 110 °C in an oven for 8 h, cooling at room temperature for one hour and then wetting under water at 23 °C for 15 h. After completion of 28 cycles of alternate wetting and drying, the changes in mass and compressive strengths of the specimens were determined. A similar exposure condition was used in previous studies to determine the durability of concrete incorporating industrial waste aggregates such as blast furnace slag and coal bottom ash (Yüksel et al. 2007; Manso et al. 2006; Aggarwal 1995). An X-ray diffraction (XRD) analysis was conducted on powdered samples in order to understand the effects of alternate cycles of high-temperature drying and wetting on the mineralogical phases. The samples were tested on powder diffractometer D8 Advance, with a copper K-alpha radiation source 40 kV and 40 mA with a Lynx Eye detector. The scan parameter was 2θ ranging from 7.5° to 90° with a step size of 0.015°. A

Table 3 Physical properties of ferronickel slag and natural sand.

Property	FNS	Sand
Density (kg/m^3)	2780	2160
Water absorption (%)	0.42	0.35
Fineness modulus	4.07	1.95

Table 4 Mix proportions of the mortars.

Sample ID	Binder (kg/m^3)			Fine aggregate (kg/m^3)		W/C
	OPC	Fly ash	GGBFS	Sand	FNS	
PC-FNS0	602	–	–	1355	0	0.47
PC-FNS25	602	–	–	1015	435	
PC-FNS50	602	–	–	678	873	
PC-FNS75	602	–	–	338	1306	
PC-FNS100	602	–	–	0	1744	
FA-FNS0	421	181	–	1355	0	
FA-FNS25	421	181	–	1015	435	
FA-FNS50	421	181	–	678	873	
FA-FNS75	421	181	–	338	1306	
FA-FNS100	421	181	–	0	1744	
BFS-FNS0	421	–	181	1355	0	
BFS-FNS25	421	–	181	1015	435	
BFS-FNS50	421	–	181	678	873	
BFS-FNS75	421	–	181	338	1306	
BFS-FNS100	421	–	181	0	1744	

qualitative phase determination was carried out by comparing the peak positions and relative intensity with the database of known crystal structure.

3. Results and Discussion

3.1 Compressive Strength Development in Normal Curing Condition

The compressive strength results at the ages of 3, 7, 28 and 56 days are presented in Fig. 4. It can be seen that compressive strength increased with increase of the percentage of FNS up to 50% in all three series of mortars and then declined with further increase of FNS. In the mortar series of 100% OPC as binder, the 28-day compressive strength gradually increased from 39 MPa for 0% FNS to 57 MPa for 50% FNS and then gradually decreased to 44 MPa for 100% FNS. While strength declined for the FNS contents beyond 50%, the compressive strength for 100% FNS was still higher than that for 100% natural sand. The trends of compressive strength variation with increase of FNS are similar at the ages of 3, 7, 28, and 56 days. Thus, the strength increase for 50% FNS and 100% FNS were 46% and 12%, respectively, as compared to the strength of the

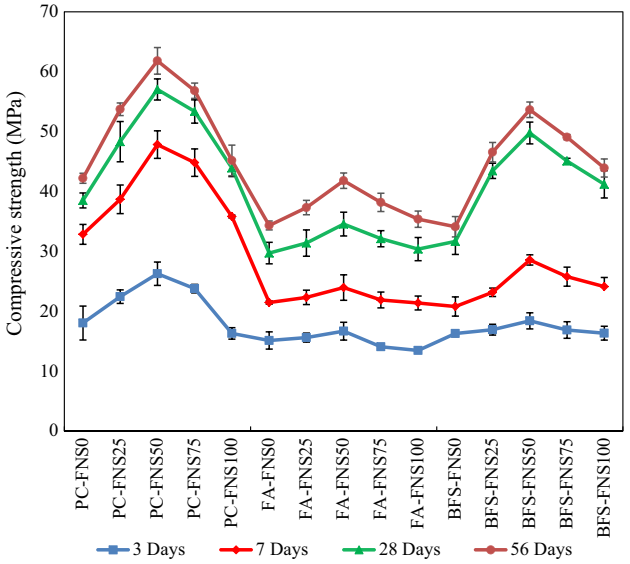

Fig. 4 Compressive strength development of mortar mixtures (error bars are at one standard deviation).

mortar with 100% natural sand. The increase of compressive strength by the inclusion of FNS is attributed to its high density and angular shape as compared to the round shape of

natural sand. The increase of FNS content improved particle packing as well as density of the samples. The improved packing and interlocking by the high density FNS particles have contributed to the increase of compressive strength. Compressive strength then declined with further increase in the FNS percentage. Therefore, 50% FNS showed the effect of maximising the strength development of mortar. This is attributed to the well-graded combination of fine aggregates, as shown in Fig. 3. The decline of compressive strength for FNS contents beyond 50% is considered to be because of reduced fine particles in the aggregate combination, as shown by the grading curves for 75 and 100% FNS (Saha and Sarker 2017b, c).

The effect of FNS on strength development of the mortar series containing 30% fly ash or 30% GGBFS is seen to be similar to that of the series containing 100% OPC as binder. The 28-day compressive strengths of the fly ash mortar with 0, 50 and 100% FNS were 30, 35 and 30 MPa respectively. Thus, strength of the mortar with 100% FNS was same as that of the mortar with 100% natural sand, whereas strength of the mortar with 50% FNS was 16% higher than that of the mortar with 100% natural sand. In the mortar series containing 30% GGBFS, the 28-day compressive strengths were 32, 50, and 41 MPa for 0, 50 and 100% FNS, respectively. Thus, compressive strength increased by 56 and 28% by replacing 50 and 100% natural sand, respectively.

When the strength developments of mortars in three series are compared, as expected, the highest strengths were observed in the series of 100% OPC as binder and the lowest strengths were observed in the series with 30% cement replacement by fly ash. In addition, the mortars in the series of 30% GGBFS as exhibited higher strengths than the mortars with 30% fly ash. This is attributed to the higher CaO content of GGBFS than fly ash. It can be seen from Fig. 4 that the lowest 3-day strength occurred in the mortar series containing 30% fly ash. However, the rate of strength development at later ages was higher in this series than the mortars of other two series, in particular between the ages of 28 and 56 days. The percentages of strength increase between 28 and 56 days in the mortars containing 50% FNS were 8, 20 and 8% for the binder series of 100% OPC, 30% fly ash and 30% GGBFS, respectively. The higher late-age strength gain of the fly ash mortar is because of the continued pozzolanic reaction of fly ash. It should be noted that though fly ash and GGBFS reduced the compressive strength, it is important to use these supplementary binders as a cement replacement in order to reduce the potential ASR expansion of FNS aggregate. The effectiveness of supplementary cementitious materials to reduce the potential ASR expansion of FNS aggregate was demonstrated by accelerated mortar bar test (AMBT) results. It was found that low-calcium fly ash was more effective to reduce the potential ASR expansion of FNS than using GGBFS. Also, it can be seen from Fig. 4 that continued pozzolanic reaction of fly ash is further demonstrated at 56 days since the compressive strength of mortars with 30% fly ash and 50% FNS reached the same level of compressive strength as mortars with 100% OPC and 100% natural sand. Therefore, the strength developments of three series of mortars presented in Fig. 4 can be used in the selection of binder and aggregate combination when using this FNS fine aggregate.

3.2 Volume of Permeable Voids (VPV)

The porosity of mortar specimens was evaluated by measuring the volume of permeable voids (VPV). The interconnected void space such as capillary pores, gel pores, air voids and microcracks can be measured by this test (Andrews-Phaedonos 2008). This test provides an indication of the ease of water penetration in concrete. The test results are plotted in Fig. 5. It can be seen that porosity of the samples increased with the increase of FNS content for all three binder groups. The highest values of VPV were observed in the mortar series of 100% cement as binder (PC-FNS series). The values of VPV were 15, 17, 18, 19 and 19% for 0, 25, 50, 75 and 100% FNS, respectively. Thus, VPV increased by about 18% by the use of 50% FNS. This increase of VPV is attributed to the increase of pores in the mortar by larger and angular FNS particles. It can be seen from Fig. 5 that the inclusion of fly ash and GGBFS in the binder has reduced the VPV values of mortar specimens. In the mortar series with 30% GGBFS (BFS-FNS series), VPV increased from 14 to 17% with the increment of FNS aggregates. Similarly, in the mortar series of 30% fly ash (FA-FNS series), VPV increased from 12 to 15% due to the use of FNS aggregates. The reduced VPV by fly ash and GGBFS is attributed to the higher fineness and pozzolanic reactions of the SCMs. The reduction of permeability of paste by inclusion of SCMs is well documented in literature (Osborne 1999; Bijen 1996; Shehata et al. 1999). However, the results of Fig. 5 show that fly ash was more effective than GGBFS in reducing VPV of the mortar specimens. The greater effectiveness of fly ash over GGBFS is attributed to its higher silica content. As shown in Table 1, silica content of the fly ash used in this study was 76% as compared to 32% in GGBFS. The higher silica content of fly ash can produce more C–S–H gel as a result of pozzolanic reaction and reduce porosity. Therefore, the fly ash mortar specimens exhibited lower VPV as compared to the GGBFS specimens.

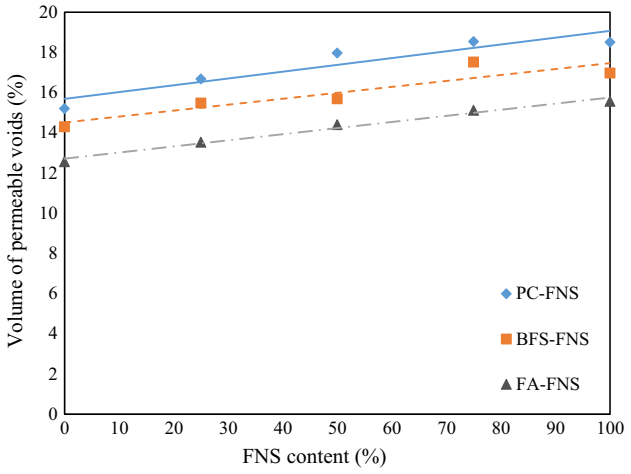

Fig. 5 Relationship between volume of permeable voids and FNS content.

Also, with 50% sand replacement by FNS, mortars using 30% fly ash or GGBFS either improved VPV or kept it at the same level as it was with 100% OPC mortars with natural sand.

3.3 Effect of Wet–Dry Cycles

3.3.1 Strength and Mass Changes by the Wet–Dry Cycles

The specimens were exposed to 28 cycles of 15 h of wetting in water following by 8 h of oven drying at 110 °C. Typical images of the specimens of PC-FNS series containing 100% FNS aggregate before and after the wet–dry cycles are shown in Fig. 6. No visible signs of cracking or damage were found in any of the specimens after the wet–dry cycles. However, some thin whitish deposit was observed on the surface after the wet–dry cycles. This thin deposit on the surface is believed to be caused by leaching out of some hydrated product from inside of the specimens. The compressive strengths after 28 cycles of alternate wetting and drying are shown in Fig. 7. The 56-day compressive strengths of the specimens in normal condition are also plotted in these figures for comparison. The effects of possible damages in the specimens by cycles of thermal expansions and contractions, as well as the cycles of moisture movement and shrinkage are considered to reflect in the compressive strengths.

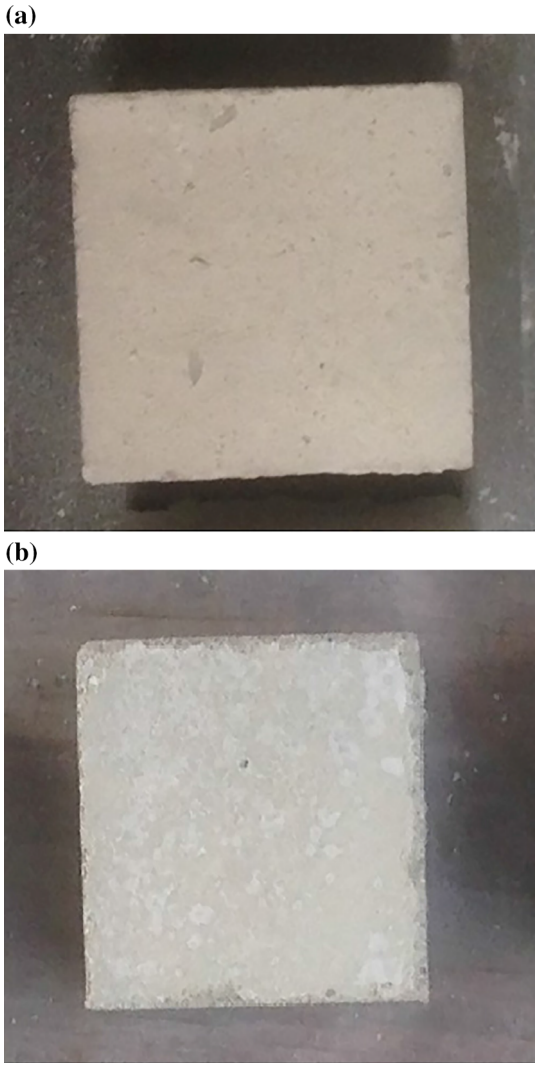

Fig. 6 (a) PC-FNS100 before wet–dry cycles and (b) PC-FNS100 after wet–dry cycles.

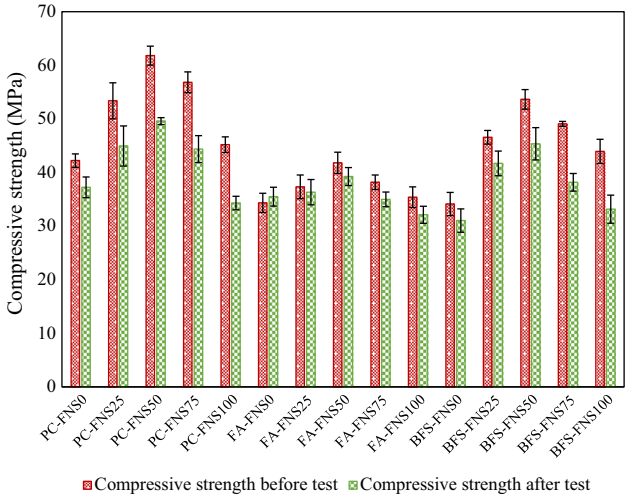

Fig. 7 Compressive strength comparison before and after wet–dry cycles (error bars are at one standard deviation).

Figure 8 shows the percentage changes of compressive strength after completion of the wet–dry cycles for various proportions of FNS aggregate. It can be seen that the control specimen with no SCM and 100% natural sand (PC-FNS0) had a strength loss of 12% after the wet–dry cycles. The strength losses of the other mortar specimens with no SCM were 16, 20, 22 and 24% for 25, 50, 75 and 100% FNS aggregate, respectively. Thus, strength loss of the specimens with no SCM increased from 12 to 24% due to complete replacement of natural sand by FNS aggregate. Similar reductions of strength by wet–dry cycles were also observed by other researchers using different types of manufactured fine aggregates. A previous study by Manso et al. (2006) reported 30–50% strength loss of concrete containing EAF slag aggregate after exposure to wet–dry cycles. Another study by Yüksel et al. (2007) reported 20–40% strength loss

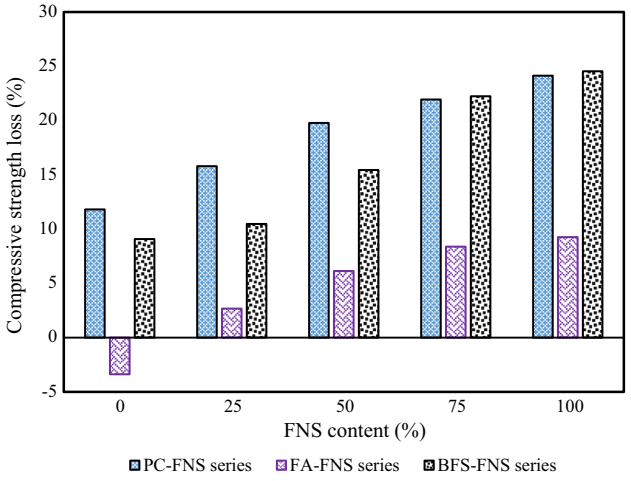

Fig. 8 Relative strength loss after wet–dry cycles for different FNS contents.

by 25 cycles of alternate wetting and drying using blast furnace slag and bottom ash as fine aggregates. Therefore, it can be said that the FNS aggregates used in this study showed better performance than EAF, blast furnace slag and bottom ash fine aggregates in the exposures of wet–dry cycles. The increased volume of permeable voids by FNS aggregate, as shown in Fig. 5, can increase the penetration of water into the specimens. The higher water penetration can cause higher vapour pressure in the specimen and result in higher strength loss, as shown in Fig. 8.

The observed strength loss by wet–dry cycles is attributed to three primary reasons. Firstly, thermal expansion and contraction by alternate heating and cooling cycles may develop internal micro-cracks. Secondly, the vapour pressure in the drying period may cause some internal damages. Thirdly, leaching out of some hydrated product by alternate wet–dry cycles, as shown by the thin surface deposit in Fig. 6, may weaken the bond between binder matrix and aggregate. The combination of these effects is considered to cause the observed strength loss of specimens after the wet–dry cycles.

As shown in Figs. 6 and 7, the trend of strength loss in the mortar series with 30% GGBFS were similar to those of the specimens with no SCM. The values of strength loss in the specimens of this series varied from 9% for no FNS to 24% for 100% FNS. On the other hand, the mortar mixes with 30% fly ash showed less strength loss after the wet–dry cycles. In fact, there was an increase of strength by 3.38% in the specimens containing 100% natural sand and no FNS aggregate. The strength losses were 2.67, 6.13, 8.38, and 9.26% for the specimens containing 25, 50, 75 and 100% FNS fine aggregate, respectively. The increase of compressive strength for the specimens without FNS aggregate was because of the pozzolanic reaction of fly ash during the cycles of wetting and drying. The availability of moisture and high-temperature (110 °C) during the exposure period accelerated the pozzolanic reaction of fly ash causing less strength loss in the specimens containing FNS aggregate. In addition, the strength loss due to wet–dry cycle is also related to the porosity and water absorption of the samples. The samples with lower porosity and water absorption exhibited less strength loss due to wet–dry cycles. The volume of permeable voids was reduced by fly ash, as shown in Fig. 5. This resulted in less strength loss after wet–dry cycles of the specimens with fly ash as compared to the specimens of other two binder series. With 50% sand replacement by FNS, mortars using 30% of GGBFS showed strength loss of the same order as it was for the 100% OPC mortars with natural sand. On the other hand, mortars using 30% fly ash showed a large improvement of strength loss as compared to the 100% OPC mortars with natural sand.

The mass loss values during the wet–dry cycle are presented in Fig. 9. It can be seen that mass loss increased almost linearly with the increase of FNS content for all three binder series. The mass loss varied from 4% to 6.2% and the trends were similar to those of strength loss. An increase of mass loss by about 30% was observed in a binder series for the use of 100% FNS aggregate as compared to that with 100% natural sand.

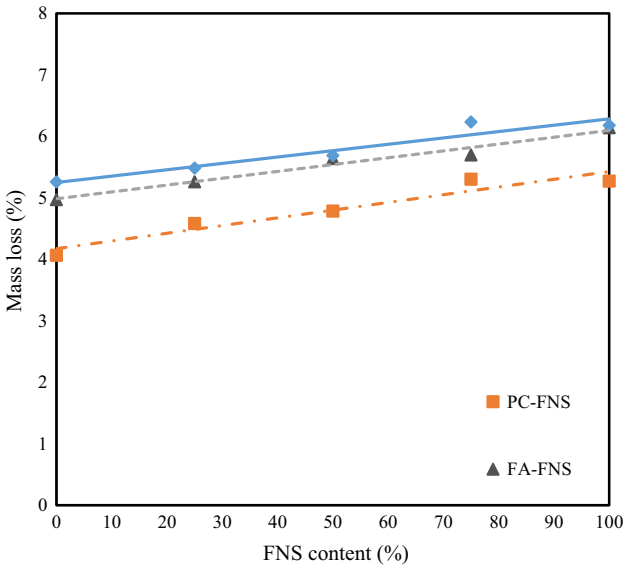

Fig. 9 Mass loss due to wet–dry cycles.

3.3.2 XRD Phases After the Wet–Dry Cycles

The mineralogical phases of mortar specimens were determined by XRD analysis after the wet–dry cycles. The XRD pattern of the mortar with no SCM and no FNS (PC-FNS0) is presented in Fig. 10a. It can be seen that the specimens of PC-FNS0 had a high amount of crystalline minerals and the majority of them was quartz (SiO_2). In addition, small amounts of portlandite ($Ca(OH)_2$), zeolite ($NaAlSi_2O_6Br{\cdot}(H_2O)_2$) and biotite ($K(MgFe)_3AlSi_3O_{10}{\cdot}(OH)_2$) were observed in the phase analysis. Quartz mineral is known for its chemical inertness and high resistance to mechanical weathering. For this reason, the specimens containing 100% natural sand had comparatively less strength and mass losses after the wet–dry cycles as compared to the specimens containing different percentages of FNS aggregate.

Figure 10b presents the XRD pattern of a specimen containing 100% FNS aggregate and no SCM (PC-FNS100). It can be seen that this specimen contained a significant amount of amorphous minerals. Furthermore, there was a significant decrease in the intensity of quartz phase as compared to the specimens with 100% natural sand. Moreover, a considerable number of peaks containing forsterite (Mg_2SiO_4), forsterite hydrous ($Mg_2SiO_3{\cdot}OH$), forsterite ferroan ($MgFeSiO_4$), forsterite hydrous ferron ($MgFeSiO_3{\cdot}OH$) and andradite ($Ca_3Fe_2Si_3O_{12}$) can be observed. These phases were originated from FNS. The forsterite ferroan has an affinity to attract hydroxyl ion and form forsterite hydrous and forsterite hydrous ferroan. Thus, during the wetting cycles, the FNS mortar samples absorbed a higher amount of water that increased vapour pressure in the drying cycle. As a consequence, strength loss of the specimens increased by the addition of FNS aggregate, as shown in Fig. 8.

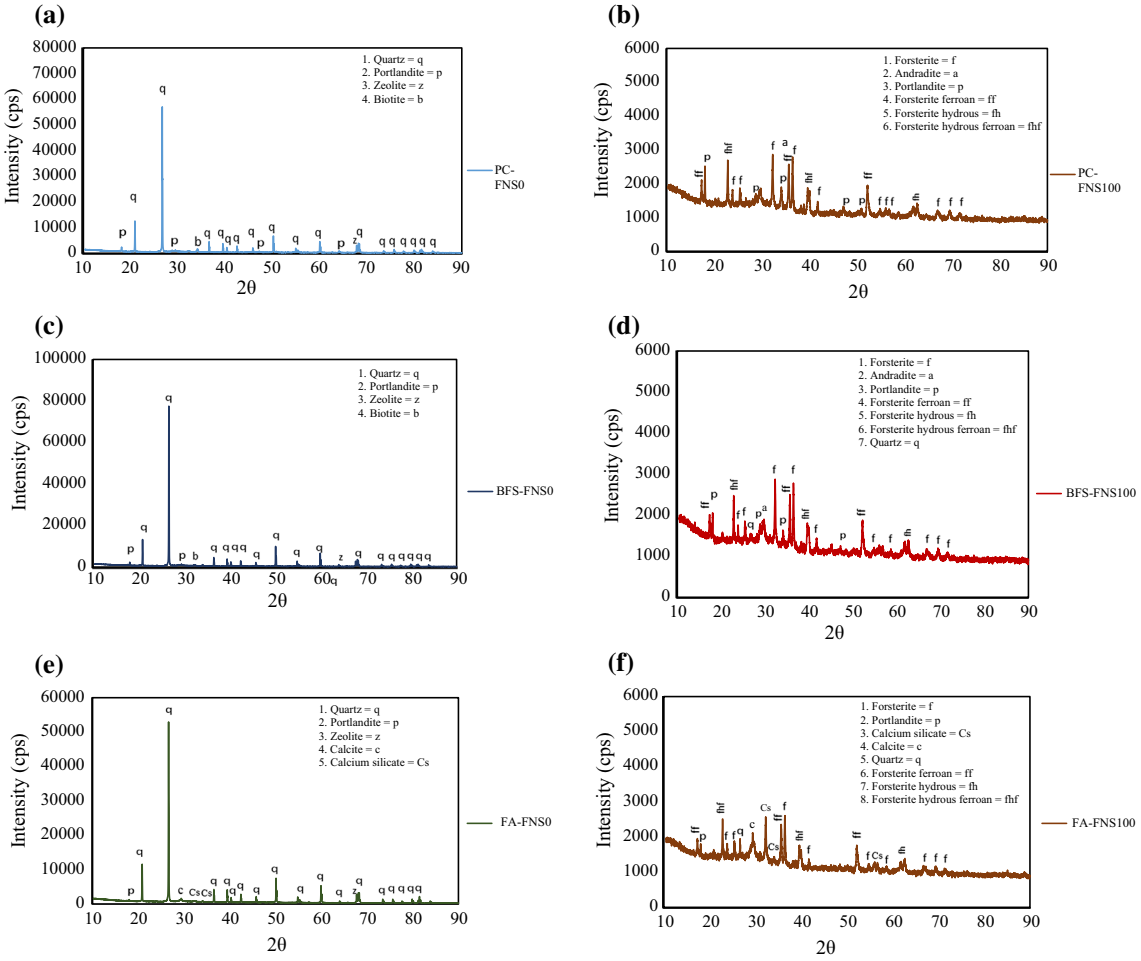

Fig. 10 XRD patterns of **a** PC-FNS0, **b** PC-FNS100, **c** BFS-FNS0, **d** BFS-FNS100, **e** FA-FNS0, and **f** FA-FNS100.

The XRD plot of a specimen with 30% GGBFS and 100% natural sand (BFS-FNS0) is shown in Fig. 10c. It can be seen that the main minerals of these samples are quartz, portlandite, zeolite and biotite, which are similar to those of the PC-FNS0 samples. There were prominent peaks of portlandite analogous to the samples of PC-FNS series. These high peaks of portlandite is an indicator of relatively less pozzolanic reaction of GGBFS than fly ash, as shown by the strengths in Fig. 6.

The XRD plot of the specimen with 30% GGBFS and 100% FNS (BFS-FNS100) is presented in Fig. 10d. It can be seen that the samples were composed of forsterite, forsterite ferroan, forsterite hydrous, forsterite hydrous ferroan, andradite, portlandite, and quartz. As expected, the majority of the peaks consisted of forsterite from FNS aggregates. Again, the high portlandite peaks indicate relatively less pozzolanic reaction of GGBFS. As a result, the strength loss of these specimens was similar to the samples with 100% OPC.

Figure 10e shows the XRD pattern of the specimen with 30% fly ash as SCM and 100% natural sand (FA-FNS0). A significant reduction in the intensity of portlandite peaks can be seen in this XRD pattern as compared to that of the specimen with 100% OPC shown in Fig. 10a. Besides, formation of calcite ($CaCO_3$) and calcium silicate (Ca_2O_4Si) is also noticeable in the XRD data. The formation calcium silicate indicates the considerable pozzolanic reaction of fly ash. The calcium silicate absorbs moisture and generated amorphous calcium silicate hydrate (C–S–H). The reaction can be generalised as Eqs. 1 and 2.

$$Ca(OH)_2 + H_4SiO_4 \rightarrow CaH_2SiO_4 + 2H_2O \quad (1)$$

$$CaH_2SiO_4 + 2H_2O \rightarrow CaH_2SiO_4 \cdot 2H_2O \quad (2)$$

The formation of calcium silicate hydrate ($CaH_2SiO_4{\cdot}2H_2O$) as a product of the pozzolanic reaction is known to increase compressive strength. Which is the primary reason for strength improvement of the specimen FA-FNS0, as shown in Fig. 7.

The XRD results of a sample with 30% fly ash and 100% FNS as aggregate (FA-FNS100) is presented in Fig. 10f. The phases of forsterite, forsterite ferroan, forsterite hydrous, forsterite hydrous ferroan, andradite, portlandite, calcium silicate and calcite can be seen in the XRD. The majority of minerals are forsterite due to 100% FNS aggregate of the specimen. Again, the XRD plot shows the formation of C–S–H, which is an indicator of the pozzolanic reaction of fly ash. As a consequence, less strength loss as compared to other two binder series was observed, as shown in Fig. 8.

In summary, the cycles of alternate wetting and drying at a high temperature (110 °C) favoured pozzolanic reaction of fly ash that resulted in strength improvement of specimens, as shown in Fig. 7. However, the use of FNS aggregate caused internal damages of specimens subjected to alternate wetting and drying.

4. Conclusion

By-product FNS was used as 25–100% replacement of natural sand with 30% fly ash or GGBFS as SCM. The strength and mass changes of mortar specimens subjected to an accelerated weathering condition was studied as an indicator of the long-term durability. The accelerated condition consisted of 28 cycles of alternate drying at 110 °C for 8 h and wetting under water at 23 °C for 15 h. The following conclusions are drawn from the study:

1. The maximum 28-day compressive strength was achieved for mortar using 50% FNS as replacement of natural sand.
2. The volume of permeable voids varied from 12 to 19% showing an increasing trend with the increase of FNS content. However, VPV decreased with the use of SCM.
3. The alternate wet–dry cycles reduced strength of all the specimens except an increase for the mortar containing 100% natural sand and 30% fly ash. The mass loss varied from 4% to 6% showing a similar trend of the strength loss.
4. The losses of strength and mass are considered to be mainly because of alternate thermal expansions and contractions, shrinkage and swelling and internal vapour pressure.
5. As evidenced by XRD, use of fly ash compensated some losses of strength by improving the volume of permeable voids through pozzolanic reaction.
6. Therefore, the use of FNS as a partial replacement of natural sand together with an SCM can be considered as a potential application of this by-product in cement mortar.

Acknowledgements

The authors acknowledge the contribution and support of SLN through its research department.

Open Access

References

Aggarwal, L. K. (1995). Bagasse-reinforced cement composites. *Cement & Concrete Composites, 17*(2), 107–112.

Aggarwal, P., Aggarwal, Y., & Gupta, S. M. (2007). Effect of bottom ash as replacement of fine aggregates in concrete. *Asian Journal of Civil Engineering, 8*(1), 49–62.

Al-Jabri, K. S., Al-Saidy, A. H., & Taha, R. (2011). Effect of copper slag as a fine aggregate on the properties of cement mortars and concrete. *Construction and Building Materials, 25*(2), 933–938.

Al-Negheimish, A. I., & Al-Zaid, R. Z. (1997). Utilization of local steel making slag in concrete. *Journal of King Saud University, 9*(1), 39–55.

Andrews-Phaedonos, F. (2008, July). Test methods for the assessment of durability of concrete. In *ARRB conference, 23rd, 2008*, Adelaide, South Australia, Australia.

AS 2758.1. (1998). *Aggregates and rock for engineering purposes*. Standards Australia. Retrieved from, http://www.siaglobal.com.

ASTM C 642. (2006). *Standard test method for density, absorption, and voids in hardened concrete*. West Conshohocken, PA: American Society for Testing and Materials (ASTM).

Ayano, T., & Sakata, K. (2000). Durability of concrete with copper slag fine aggregate. *Special Publication, 192,* 141–158.

Bai, Y., Darcy, F., & Basheer, P. A. M. (2005). Strength and drying shrinkage properties of concrete containing furnace bottom ash as fine aggregate. *Construction and Building Materials, 19*(9), 691–697.

Bijen, J. (1996). Benefits of slag and fly ash. *Construction and Building Materials, 10*(5), 309–314.

Brindha, D., & Nagan, S. (2011). Durability studies on copper slag admixed concrete. *Asian Journal of Civil Engineering (Building and Housing), 12*(5), 563–578.

Choi, Y. C., & Choi, S. (2015). Alkali–silica reactivity of cementitious materials using ferro-nickel slag fine aggregates produced in different cooling conditions. *Construction and Building Materials, 99,* 279–287.

Davis, J., Bird, J., Finlayson, B., & Scott, R. (2000). The management of gravel extraction in alluvial rivers: a case study from the Avon River, southeastern Australia. *Physical Geography, 21*(2), 133–154.

Etxeberria, M., Pacheco, C., Meneses, J. M., & Berridi, I. (2010). Properties of concrete using metallurgical industrial by-products as aggregates. *Construction and Building Materials, 24*(9), 1594–1600.

Ghafoori, N., & Bucholc, J. (1996). Investigation of lignite-based bottom ash for structural concrete. *Journal of Materials in Civil Engineering, 8*(3), 128–137.

Hooton, R. D. (2000). Canadian use of ground granulated blast-furnace slag as a supplementary cementing material for enhanced performance of concrete. *Canadian Journal of Civil Engineering, 27*(4), 754–760.

JMIA. (1991). Research of ferronickel slag fine aggregate for concrete. *Japan Mining Industry Association*. Retrieved from, http://jglobal.jst.go.jp.

JSCE Committee. (1994). Guidelines for construction using Ferronickel slag fine aggregate concrete. *Concr. Libr. JSCE*. 24 Retrieved from May 20, 2015, from http://www.jsce.or.jp

Kang, S. S., Park, K., & Kim, D. (2014). Potential soil contamination in areas where ferronickel slag is used for reclamation work. *Materials, 7*(10), 7157–7172.

Kim, J. E., Park, W. S., Jang, Y. I., Kim, S. W., Kim, S. W., Nam, Y. H., et al. (2016). Mechanical properties of energy efficient concretes made with binary, ternary, and quaternary cementitious blends of fly ash, blast furnace slag, and silica fume. *International Journal of Concrete Structures and Materials, 10*(3), 97–108.

Manso, J. M., Gonzalez, J. J., & Polanco, J. A. (2004). Electric arc furnace slag in concrete. *Journal of Materials in Civil Engineering, 16*(6), 639–645.

Manso, J. M., Polanco, J. A., Losanez, M., & González, J. J. (2006). Durability of concrete made with EAF slag as aggregate. *Cement & Concrete Composites, 28*(6), 528–534.

Maslehuddin, M., Sharif, A. M., Shameem, M., Ibrahim, M., & Barry, M. S. (2003). Comparison of properties of steel slag and crushed limestone aggregate concretes. *Construction and Building Materials, 17*(2), 105–112.

Osborne, G. J. (1999). Durability of Portland blast-furnace slag cement concrete. *Cement & Concrete Composites, 21*(1), 11–21.

Padmalal, D., Maya, K., Sreebha, S., & Sreeja, R. (2008). Environmental effects of river sand mining: a case from the river catchments of Vembanad lake, Southwest coast of India. *Environmental geology, 54*(4), 879–889.

Pellegrino, C., & Gaddo, V. (2009). Mechanical and durability characteristics of concrete containing EAF slag as aggregate. *Cement & Concrete Composites, 31*(9), 663–671.

Preciso, E., Salemi, E., & Billi, P. (2012). Land use changes, torrent control works and sediment mining: Effects on channel morphology and sediment flux, case study of the Reno River (Northern Italy). *Hydrological Processes, 26*(8), 1134–1148.

Qasrawi, H., Shalabi, F., & Asi, I. (2009). Use of low CaO unprocessed steel slag in concrete as fine aggregate. *Construction and Building Materials, 23*(2), 1118–1125.

Rahman, M. A., Sarker, P. K., Shaikh, F. U. A., & Saha, A. K. (2017). Soundness and compressive strength of Portland cement blended with ground granulated ferronickel slag. *Construction and Building Materials, 140,* 194–202.

Roychand, R., De Silva, S., Law, D., & Setunge, S. (2016). Micro and nano engineered high volume ultrafine fly ash cement composite with and without additives. *International Journal of Concrete Structures and Materials, 10*(1), 113–124.

Safiuddin, M., Jumaat, M. Z., Salam, M. A., Islam, M. S., & Hashim, R. (2010). Utilization of solid wastes in construction materials. *International Journal of Physical Sciences, 5*(13), 1952–1963.

Saha, A. K., & Sarker, P. K. (2016). Expansion due to alkali-silica reaction of ferronickel slag fine aggregate in OPC and blended cement mortars. *Construction and Building Materials, 123,* 135–142.

Saha, A. K., & Sarker, P. K. (2017a). Sustainable use of ferronickel slag fine aggregate and fly ash in structural concrete: Mechanical properties and leaching study. *Journal of Cleaner Production*.

Saha, A. K., & Sarker, P. K. (2017b). Compressive strength of mortar containing ferronickel slag as replacement of natural sand. *Procedia Engineering, 171,* 689–694.

Saha, A. K., & Sarker, P. K. (2017c). Durability characteristics of concrete using ferronickel slag fine aggregate and fly ash. *Magazine of Concrete Research*. https://doi.org/10.1680/jmacr.17.00260.

Sakoi, Y., Aba, M., Tsukinaga, Y., & Nagataki, S. (2013). Properties of concrete using ferronickel slag aggregate. In *Proceedings of the 3rd international conference on sustainable construction materials and technologies*, Tokyo, Japan (pp. 1–6).

Sato, T., Watanabe, K., Ota, A., Aba, M., & Sakoi, Y. (2011). Influence of excessive bleeding on frost susceptibility of concrete incorporating ferronickel slag as aggregates. In *36th conference on our world in concrete & structures*.

Shafigh, P., Jumaat, M. Z., Mahmud, H. B., & Alengaram, U. J. (2013). Oil palm shell lightweight concrete containing high volume ground granulated blast furnace slag. *Construction and Building Materials, 40,* 231–238.

Shehata, M. H., Thomas, M. D., & Bleszynski, R. F. (1999). The effects of fly ash composition on the chemistry of pore solution in hydrated cement pastes. *Cement and Concrete Research, 29*(12), 1915–1920.

Shoya, M., Aba, M., Tsukinaga, Y., & Tokuhashi, K. (2003). Frost resistance and air void system of self-compacting concrete incorporating slag as a fine aggregate. *Special Publication, 212,* 1093–1108.

Shoya, M., Nagataki, S., Tomosawa, F., Sugita, S., & Tsukinaga, Y. (1997). Freezing and thawing resistance of concrete with excessive bleeding and its improvement. *Special Publication, 170,* 879–898.

Shoya, M., Sugita, S., Tsukinaga, Y., Aba, M., Tokuhasi, K., Dhir, R. K., & Jappy, T. G. (1999, September). Properties of self-compacting concrete with slag fine aggregates. In *Proceedings of the international seminar on exploiting wastes in concrete*, Thomas Telford (Vol. 7, pp. 121–130).

Siddique, R., & Khan, M. I. (2011). *Supplementary cementing materials*. New York: Springer.

Tomosawa, F., Nagataki, S., Kajiwara, T., & Yokoyama, M. (1997). Alkali-aggregate reactivity of ferronickel-slag aggregate concrete. *Special Publication, 170,* 1591–1602.

Wang, G., Thompson, R., & Wang, Y. (2011). Hot-mix asphalt that contains nickel slag aggregate: Laboratory evaluation of use in highway construction. *Transportation research record: Journal of the Transportation Research Board, 2208,* 1–8.

Wu, W., Zhang, W., & Ma, G. (2010). Optimum content of copper slag as a fine aggregate in high strength concrete. *Materials and Design, 31*(6), 2878–2883.

Yang, J. M., Yoo, D. Y., Kim, Y. C., & Yoon, Y. S. (2017). Mechanical properties of steam cured high-strength steel fiber-reinforced concrete with high-volume blast furnace

slag. *International Journal of Concrete Structures and Materials, 11*(2), 391–401.

Yüksel, İ., Bilir, T., & Özkan, Ö. (2007). Durability of concrete incorporating non-ground blast furnace slag and bottom ash as fine aggregate. *Building and Environment, 42*(7), 2651–2659.

Yüksel, İ., Siddique, R., & Özkan, Ö. (2011). Influence of high temperature on the properties of concretes made with industrial by-products as fine aggregate replacement. *Construction and Building Materials, 25*(2), 967–972.